ELSEVIER

Polymer 41 (2000) 5157–5164

polymer

Crystallization induced microstructure of polymer blends consisting of two crystalline constituents

Hsin-Lung Chen*, Shi-Fang Wang

Department of Chemical Engineering, National Tsing Hua University, Hsin-Chu 30043, Taiwan, ROC

Received 23 March 1999; accepted 13 September 1999

Abstract

The crystallization kinetics and semicrystalline morphology of a polymer blend consisting of two crystalline components, poly(ethylene oxide) (PEO) and poly(ethylene succinate) (PES), have been investigated. PEO and PES were miscible in the melt. Slight dilution with PEO ($w_{PEO} \leq 0.2$) promoted the crystallization kinetics of PES because of enhanced segmental mobility upon blending. Further increase in PEO content reduced the PES crystallization rate owing to the dominant effect of depression in crystallization driving force. The semicrystalline morphology of PEO/PES blends was probed by small-angle X-ray scattering (SAXS). At temperatures between the melting point of PEO ($T_m^{PEO} \approx 59$°C) and that of PES ($T_m^{PES} \approx 101$°C), the blend was a crystalline/amorphous system. Both crystallizations via direct cooling to 70°C (where only PES crystallized) and direct cooling to 40°C (where two components crystallized simultaneously) followed by heating to 68°C (to melt PEO crystals) created a high extent of interfibrillar segregation coupled with a minor extent of interlamellar incorporation of amorphous PEO. At temperatures below T_m^{PEO}, where the blend was a crystalline/crystalline system, direct cooling to 40°C (one-step crystallization) generated two separate lamellar stack (LS) domains: one containing almost pure PES lamellae and the other consisting of mixed PEO and PES lamellae. Crystallization at 70°C followed by cooling to room temperature (two-step crystallization) also yielded two separate LS domains, due to the crystallization of PEO within the interfibrillar regions.

Keywords: Poly(ethylene oxide); Poly(ethylene succinnate); Blend

1. Introduction

Based on the crystallizability of the constituents, binary polymer blends can be classified into amorphous/amorphous, crystalline/amorphous, and crystalline/crystalline systems. For the latter two systems where at least one component is crystallizable, occurrence of liquid–solid phase separation offers an effective route to produce a wide variety of morphological patterns [1]. In a melt-miscible crystalline /amorphous blend, for example, crystallization is accompanied with the segregation of the amorphous diluent. The morphological pattern is characterized by the distance over which the diluent is expelled, where three basic types of morphologies may be generated: (1) interlamellar segregation, where the diluent is expelled by a short distance such that it is trapped inside the interlamellar regions; (2) interfibrillar segregation, where the diluent is segregated by a larger distance to the regions between the lamellar bundles; (3) interspherulitic segregation, where the diluent is rejected out of the spherulites [1]. These morphological patterns represent the diluent dispersion from nanometer for interlamellar segregation to micrometer for interspherulitic segregation. Different scales of dispersion may lead to different properties.

For crystalline/crystalline systems where cocrystallization is absent, crystallization of the two components creates two crystal species (A and B). The morphology is characterized by the arrangement of the two crystal species, where the pattern can be categorized into (Fig. 1):

1. Insertion mode, where A crystals and B crystals mix in the lamellar stack. The configuration can be random (ABAABABB) or alternating (ABABAB).
2. Block mode, where A crystals and B crystals form respective lamellar stack (LS) domains. The configuration can be a sequence of pure A attached to a sequence of pure B (AAAAABBBBB, Fig. 1(c)) or a sequence of pure A connected with a sequence of mixed A and B (AAAAABBABAABBB…, Fig. 1(d)).

The formation of these morphological patterns is governed by the mutual exclusion distance of the two components

* Corresponding author. Tel.: +886-03-5721714; fax: +886-03-5715408.
E-mail address: hlchen@che.nthw.edu.tw (H.-L. Chen).

0032-3861/00/$ - see front matter
PII: S0032-3861(99)00745-4

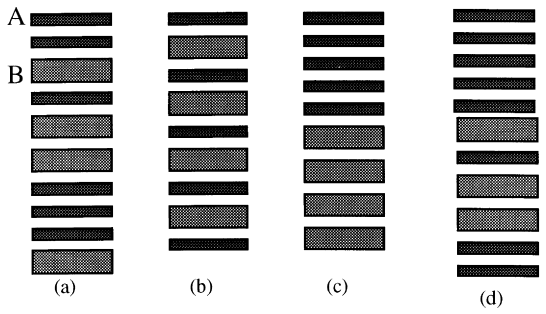

Fig. 1. Possible modes of lamellar arrangement in crystalline/crystalline blends without cocrystallization: (a) insertion mode with random arrangement; (b) insertion mode with alternating arrangement; (c) block mode with a sequence of A crystals attached with a sequence of B crystals; and (d) block mode with a sequence of A connected with a sequence of mixed A and B.

during crystallization [2,3]. Insertion mode is induced by the mutual segregation distance comparable to the lamellar thickness, which is in the order of several nm. Block mode is characterized by the longer segregation distance, in the order of tens of nm to μm.

Since mutual segregation distance is determined by the mutual diffusivity of the two components, it should be influenced by temperature, composition, and molecular weight. The morphological structure may also be controlled by thermal history. For instance, if the melting point $T_m^A > T_m^B$, the crystalline/crystalline morphology can be induced by either one-step or two-step crystallizations. One-step crystallization involves direct cooling of the blend from the melt to the crystallization temperature $(T_c) < T_m^B$; in this case the morphological pattern is governed by the mutual exclusion during simultaneous crystallization of the two components. Two-step crystallization is proceeded by cooling from the melt to $T_m^B < T_{c1} < T_m^A$ to allow crystallization of A for a period of time; the blend is subsequently cooled to $T_{c2} < T_m^B$ to allow the crystallization of B. In this case, the eventual crystalline/crystalline morphology is correlated with the crystalline/amorphous morphology created at T_{c1}. If interlamellar segregation of B occurs at T_{c1}, then the subsequent crystallization of B at T_{c2} will lead to the insertion arrangement of A and B crystals. On the other hand, if interfibrillar segregation of B takes place at T_{c1}, subsequent crystallization of B will yield the block arrangement of the two crystal species.

The morphological structure in crystalline/amorphous blends has been investigated extensively, but very limited attention has been directed to crystalline/crystalline systems. The most widely studied system is perhaps the blends of high-density polyethylene (HDPE) and low-density polyethylene (LDPE) (e.g. Refs. [4–11]). This binary pair represents an "ideal (yet complex) system" in the sense that the effect of unlike intermolecular interaction is nil. Other crystalline/crystalline blends such as polycarbonate (PC)/polycaprolactone (PCL) [2,3,12,13], poly (ethylene terephthalate) (PET)/poly(butylene terephthalate) (PBT) [1,14], poly(vinylidene fluoride) (PVDF)/poly (butylene adipate) (PBA) [15–18], poly(3-hydroxybutyrate) (PHB)/poly(ethylene oxide) (PEO) [19–21], and PBT/polyarylates (PAr) [22] have been reported. PC/PCL and PVDF /PBA are the two systems whose morphological structures have been characterized in detail. Cheung and coworkers reported the predominant insertion arrangement of PC and PCL lamellae in PC/PCL system [2,3,12,13]. On the other hand, block lamellar arrangement has been observed in PVDF/PBA blends [18].

In this paper, the crystallization kinetics and morphological pattern of a new melt-miscible crystalline/crystalline system consisting of PEO and poly(ethylene succinate) (PES) is reported. PEO and PES are both crystalline polymers with the melting points of ca. 59 and 101°C, respectively. At the temperatures between 59 and 101°C, PEO/PES is a crystalline/amorphous system, while the blend becomes a crystalline/crystalline system below 59°C. In this paper, the miscibility and crystallization kinetics of PEO/PES blends are studied by differential scanning calorimetry (DSC) and optical microscopy. The morphological structures in both crystalline/amorphous and crystalline/crystalline states are probed by means of small-angle X-ray scattering (SAXS) and are discussed as a function of thermal history.

2. Experimental section

2.1. Materials and sample preparation

PEO with molecular weight of 100,000 was purchased from Monomer–Polymer & Dajac Laboratories Inc., and PES was acquired from Aldrich. Blending of PEO and PES were carried out by solution casting. The blending components were dissolved in chloroform at room temperature yielding a 1 wt% solution. The solution was subsequently poured onto a petri dish and the blend film was obtained after evaporating most solvent on a hot plate at ca. 60°C. The blend film was further dried in vacuo at 50°C for 24 h.

Samples for SAXS study were prepared by compression molding. The blend obtained from solution casting was compression molded by a hot press at 120°C for 5 min to yield a disk of ca. 1 mm thickness. The samples were subsequently treated by either one-step or two-step crystallization. For one-step crystallization, the samples were quickly transferred from 120°C into an oven equilibrated at 40 ± 1°C for crystallization. Crystallization was conducted for 24 h. For two-step crystallization, the samples were transferred from 120°C to an oven equilibrated at 70 ± 1°C where crystallization was allowed to proceed for 24 h. The samples were subsequently cooled to room temperature (ca. 27°C) by taking the sample out of the oven to allow the crystallization of PEO.

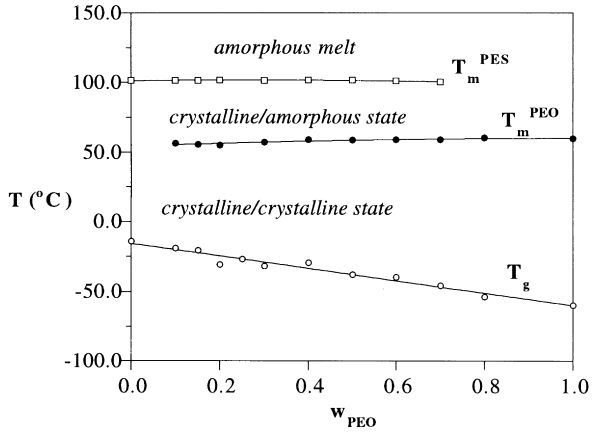

Fig. 2. T_g, T_m^{PEO} and T_m^{PES} vs. composition of PEO/PES quenched from 120°C.

2.2. Thermal transition and crystal growth rate measurements

The glass transition temperatures (T_g) and melting points of melt-quenched PEO/PES blends were measured by a TA Instrument 2000 differential scanning calorimeter (DSC). The sample was annealed at 120°C for 3 min followed by quenching into liquid nitrogen. The DSC scanning rate was 20°C/min.

The spherulite growth was monitored with a Pac Hund polarized optical microscope. The sample was first melted on a Linkam HFS91 hot stage at 120°C for 3 min. It was then quickly transferred to another hot stage equilibrated at the crystallization temperature where the spherulite growth was monitored. Micrographs were taken at intervals for measuring the spherulite radii (R) at various time periods. The growth rate was calculated from the change of spherulite radius with time, dR/dt.

2.3. SAXS measurement

The crystalline/crystalline and crystalline/amorphous morphologies were probed by SAXS performed at room temperature (ca. 27°C) and 68°C, respectively. The power of X-ray source was operated at 200 mA and 40 kV. The X-ray source is a 18 kW rotating anode X-ray generator (Rigaku) equipped with a rotating anode Cu target. The incident X-ray beam was monochromated by a pyrolytic graphite and a set of three pinhole inherent collimators were used so that the smearing effects inherent in slit-collimated small-angle X-ray cameras can be avoided. The sizes of the first and second pinhole are 1.5 and 1.0 mm, respectively, and the size of the guard pinhole before the sample is 2.0 mm. The scattered intensity was detected by a two-dimensional position sensitive detector (ORDELA Model 2201X, Oak Ridge Detector Laboratory Inc., USA) with 256×256 channels (active area 20×20 cm^2 with $\sim$1 mm resolution). The sample to detector distance is either 5000 or 2000 mm long. The beam stop is a round lead disc of 18 mm in diameter. All data were corrected by the background (dark current and empty beam scattering) and the sensitivity of each pixel of the area detector. The area scattering pattern has been radially averaged to increase the efficiency of data collection compared with one-dimensional linear detector. Data were acquired and processed on an IBM compatible personal computer. The intensity profile was output as the plot of the scattering intensity (I) versus the scattering factor, $q = 4\pi/\lambda \sin(\theta/2)$ (θ = scattering angle).

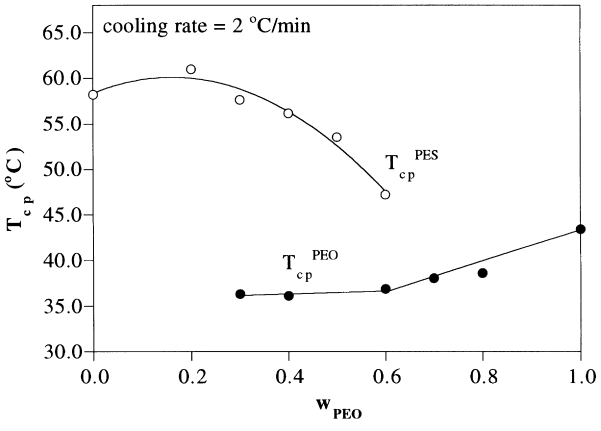

Fig. 3. Influence of composition on the exothermic peak temperatures (T_{cp}) observed from the DSC cooling exotherms at the cooling rate of 2°C/min.

3. Results and discussion

3.1. Miscibility and crystallization kinetics

The glass transition temperatures of PEO/PES blends quenched from the melt (120°C) are plotted against composition in Fig. 2. Melt miscibility of PEO/PES is established from the observation of a single composition dependent T_g over the entire composition range. Nearly all melt-quenched PEO/PES were semicrystalline prior to DSC scans. Fig. 2 also plots the observed melting points (T_m^{PEO} = melting point of PEO; T_m^{PES} = melting point of PES) against composition. Two melting peaks at ca. 59 and 101°C corresponding to the meltings of PEO and PES crystals were always observed and depressions in melting points were slight (less than 2°C for T_m^{PES} and less than 4°C for T_m^{PEO}). This means PEO and PES did not cocrystallize. In the temperature range between 59 and 101°C, where only PES can crystallize, the blend behaves as a crystalline/amorphous system. The blend becomes a crystalline/crystalline system below 59°C because both components can crystallize.

Miscibility of PEO/PES can be further established from the crystallization kinetics studies, as crystallization rates of both components are affected by the intimate mixing in the melt. Fig. 3 shows the effect of composition on the exothermic peak temperatures (T_{cp}) observed from the DSC cooling exotherms at the cooling rate of 2°C/min. The

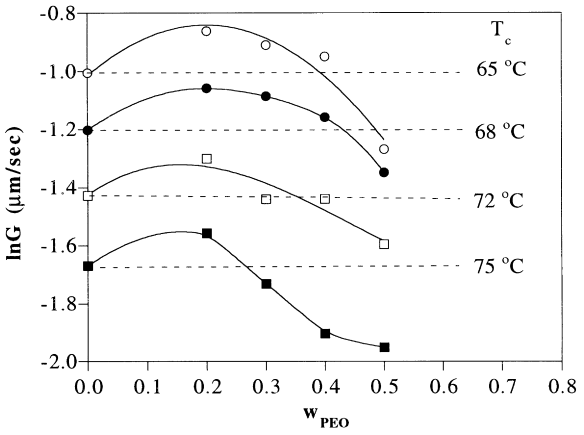

Fig. 4. Composition variations of the crystal growth rates of PES in PEO/PES blends. The crystallization temperatures are indicated in the figure.

composition dependence of T_{cp}^{PES} displays a shallow maximum at $w_{PEO} = 0.2$, indicating that the crystallization rate of PES was promoted upon blending with 20 wt% PEO but further increase in PEO content depressed the PES crystallization rate. The presence of a maximum is attributed to the competitive effect between the enhanced segmental mobility and depressed crystallization driving force upon blending with PEO. Miscibility with PEO enhances the segmental mobility of PES because of lowering in T_g, while dilution of PES as well as depression in equilibrium melting point reduce the crystallization driving force. The interplay between these two opposing effects generates a maximum in the composition dependence of the PES crystallization rate.

Blending also affects the crystallization kinetics of PEO, where the rate drops with increasing PES content but reaches approximately a constant when PES composition exceeds 40 wt%. In the cooling process, crystallization of PES took place prior to the crystallization of PEO; the existing PES crystals may act as the nucleation centers for the subsequent PEO crystallization and promoted its crystallization rate. It is likely that the counterbalance between the favorable nucleation induced by PES crystals and the dilution effect led to the rather constant PEO crystallization rate as $w_{PES} \geq 0.4$. The detailed study on isothermal crystallization kinetics, including the effect of prior PES crystallization on the crystallization rate of PEO, is currently underway.

Fig. 4 displays the effect of composition on the crystal growth rate of PES in the temperature range of 65–75°C. The plot also displays a maximum due to the interplay between mobility and driving force associated with crystallization. The dashed lines in Fig. 4 specify the growth rates of neat PES. At lower T_c of 65 and 68°C, the crystal growth rates in the blends exceed that of neat PES except for 50/50 composition. On the other hand, nearly all compositions exhibit slower growth rate except 20/80 composition at 72 and 75°C. The depression in crystallization driving force appears to play a more dominant role in controlling the crystal growth rate as T_c increases.

3.2. Morphological structure in crystalline/amorphous state

At temperatures between T_m^{PEO} and T_m^{PES}, PEO/PES is a crystalline/amorphous system where PEO simply acts as an amorphous diluent. The semicrystalline morphology is characterized by the distance over which the amorphous PEO is segregated. Fig. 5 displays the spherulite morphology of PES and the 50/50 blend viewed under polarized optical microscopy (POM) at 70°C. Spherulites of neat PES are compact but those of the 50/50 blend exhibit more opened texture. Since the spherulites are volume filling, the observed morphology may indicate the exclusion of PEO into the interfibrillar regions. Cooling from 70 to 40°C compacted the spherulites due to crystallization of PEO within the interfibrillar regions (Fig. 5(c)).

The crystalline/amorphous morphology is further elucidated by SAXS experiments performed at 68°C. Samples were treated by two types of thermal history. The first involved direct cooling from melt to 70°C to allow PES crystallization. In this case, morphology was governed by the segregation of amorphous PEO during PES crystallization. The other thermal history involved direct cooling to 40°C followed by heating to 68°C to conduct the SAXS experiments. In this case, the morphology was governed by the mutual exclusion of PEO and PES during simultaneous crystallization at 40°C.

Fig. 6 displays the high-temperature (68°C) Lorentz-corrected SAXS profiles of the blends treated by both

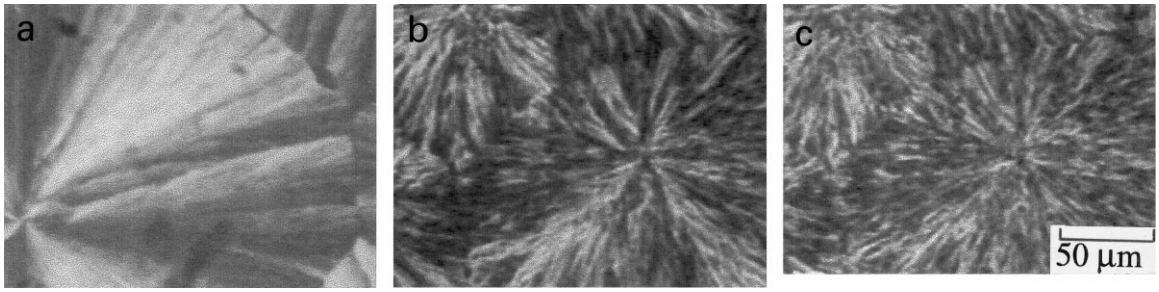

Fig. 5. Polarized optical micrographs showing the spherulite morphology of: (a) PES at 70°C; (b) PEO/PES 50/50 blend at 70°C; and (c) 50/50 blend cooled from 70 to 40°C.

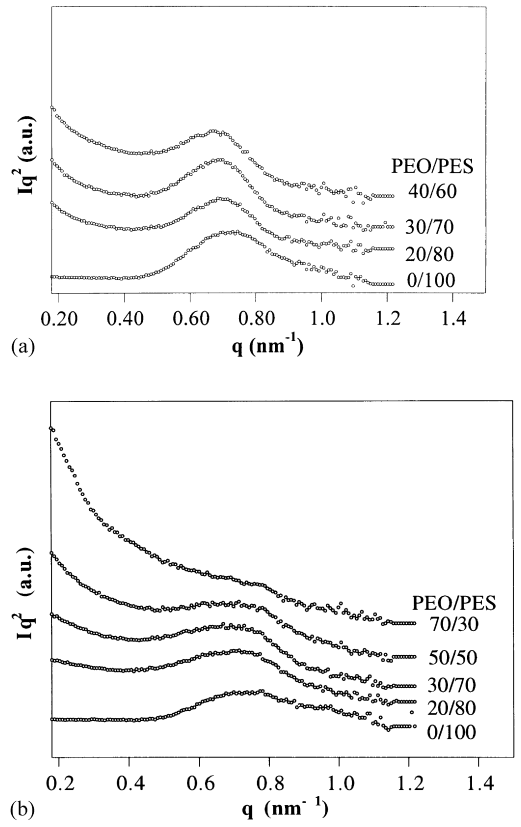

Fig. 6. High-temperature (68°C) Lorentz-corrected SAXS profiles of PEO/PES. Thermal histories are: (a) direct cooling from the melt to 70°C; and (b) direct cooling to 40°C followed by heating to 68°C.

thermal histories. Neat PES exhibits a typical scattering peak associated with the electron density contrast between the alternating crystalline and amorphous layers. PEO/PES blends display very different scattering patterns. For both thermal histories, the scattering intensity increases abruptly at the low angular region. The overall scattering patterns are characterized by the superposition of a monotonically decayed profile and a scattering peak associated with PES lamellar stacks. The large low-q intensity or "zero-angle scattering" signifies the presence of a heterogeneity having the size larger than the crystalline and amorphous layers. This type of zero-angle scattering has been observed in crystalline/amorphous blends such as PBT/PAr [23] and isotactic-PHB/atactic-PHB [24] where the morphology was induced by liquid–solid phase separation, and in PCL/polystyrene oligomer (PSO) [25,26] and PET/poly (ether imide) [27] where morphology was induced by combined crystallization and liquid–liquid demixing. According to Schultz [28], the zero-angle scattering may be attributed to a large (greater than lamellar length scales) individual amorphous domain inserted into the stacks of several lamellae and creating a gap in the lamellar stacks. The electron density contrast between this large amorphous domain and the lamellar stack domain (LS domains) consisting of alternating crystalline–amorphous layers gives rise to the zero-angle scattering [25–27]. In PEO/PES blends, the large amorphous domains exterior to the PES LS domains are the interfibrillar regions formed by the extralamellar segregation of PEO. These exterior amorphous domains were generated as PEO was segregated beyond several layers of lamellae. The zero-angle scattering provides further evidence to the extralamellar segregation of PEO.

The zero-angle scattering is modeled by the Debye–Bueche equation which is generally applicable to the scattering from random structured two-phase systems. The scattering intensity is given by [29]

$$I(q) = \frac{A}{(1 + a_c^2 q^2)^2}$$

where A is a constant and a_c the correlation length which is a measure of the size of heterogeneity. Fig. 7 shows the Debye–Bueche plots ($I^{-1/2}$ vs. q^2) of PEO/PES blends. Good linearity is observed at low-q region, signifying the applicability of the Debye–Bueche model. Deviation from the initial linearity occurs at $q \approx 0.18\ \mathrm{nm}^{-1}$ owing to the scattering contribution of PES LS domains. Table 1 lists the correlation lengths deduced from the Debye–Bueche plots. The average correlation length of the blends treated by direct cooling to 40°C is 8.8 nm whereas crystallization at 70°C yielded the average a_c of 24.6 nm, about 1.8 times larger. Larger correlation length implies larger LS and exterior amorphous domains were created by crystallization at 70°C.

The morphological formation via simultaneous crystallization at 40°C deserves further attention. In this case, the disparity in crystallization kinetics of the constituents can be a governing factor for the morphological structure, besides the intrinsic diffusivity associated with the mutual exclusion of the amorphous chains of the two components. When both components crystallize with a comparable rate, the mutual segregation distance should be minimized and the lamellar arrangement approaches the insertion mode. For PEO/PES blends crystallized at 40°C, it was observed from POM that PEO and PES crystallized at different rates from the miscible melt. The onset of PES crystallization preceded the onset of PEO crystallization due to the much larger degree of supercooling which induced a faster nucleation rate. It can be postulated that there existed a time period over which PEO was a "temporary amorphous diluent" with respect to PES. This "temporary amorphous diluent" was segregated beyond the lamellar distance, leading to the interfibrillar morphology, and subsequent crystallization would create the block lamellar arrangement.

Although the presence of zero-angle scattering verifies the extralamellar segregation of PEO, it does not preclude the possibility of partial interlamellar incorporation. Interlamellar segregation was revealed by computing the long period associated with the PES LS domains from the scattering peak (q_{max}) using the Braggs equation ($L = 2\pi/q_{max}$). The results are plotted against composition in

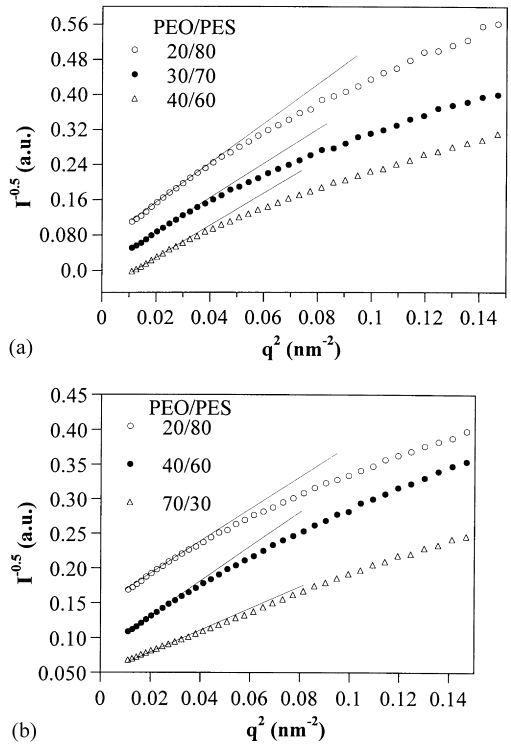

Fig. 7. Debye–Bueche plots of crystalline/amorphous PEO/PES blends. Thermal histories are: (a) direct cooling from the melt to 70°C; and (b) direct cooling to 40°C followed by heating to 68°C.

Fig. 8. The long period increases slightly by ca. 0.5 nm upon blending with 30 wt% PEO, but the composition variation appears to level off with further increase in PEO content. Rise in long period may imply the swelling of amorphous layers and hence partial interlamellar incorporation of PEO. However, the extent of interlamellar segregation is very minor, particularly for the composition of $w_{PEO} > 0.3$, as the majority of PEO was expelled interfibrillarly.

3.3. Morphological structure in crystalline/crystalline state

Since the blends in crystalline/amorphous state exhibited large extent of interfibrillar segregation, subsequent crystallization of PEO upon cooling to $T_c < T_m^{PEO}$ should predominantly occur in the interfibrillar regions, creating a separate LS domain. Fig. 9 displays the room-temperature

Table 1
Debye–Bueche correlation lengths (a_c) of PEO/PES blends in the crystalline/amorphous state

w_{PEO}	a_c (nm)[a]	a_c (nm)[b]
0.2	26.5	7.9
0.3	25.2	8.5
0.4	22.0	11.1
0.5		9.0
0.7		7.8

[a] Direct cooling to 70°C.
[b] Direct cooling to 40°C followed by heating to 68°C.

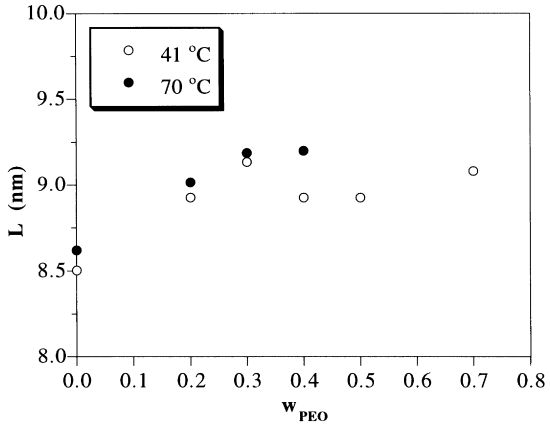

Fig. 8. Variations of long period with composition for PEO/PES blends. Thermal histories are: direct cooling from the melt to 70°C (filled symbol); and direct cooling to 40°C followed by heating to 68°C (open symbol).

Lorentz-corrected SAXS profiles of PEO/PES subjected to: (a) two-step crystallization, where the blends were isothermally crystallized at 70°C for 24 h followed by cooling to room temperature (ca. 27°C) to allow PEO crystallization; and (b) one-step crystallization, where the blends were

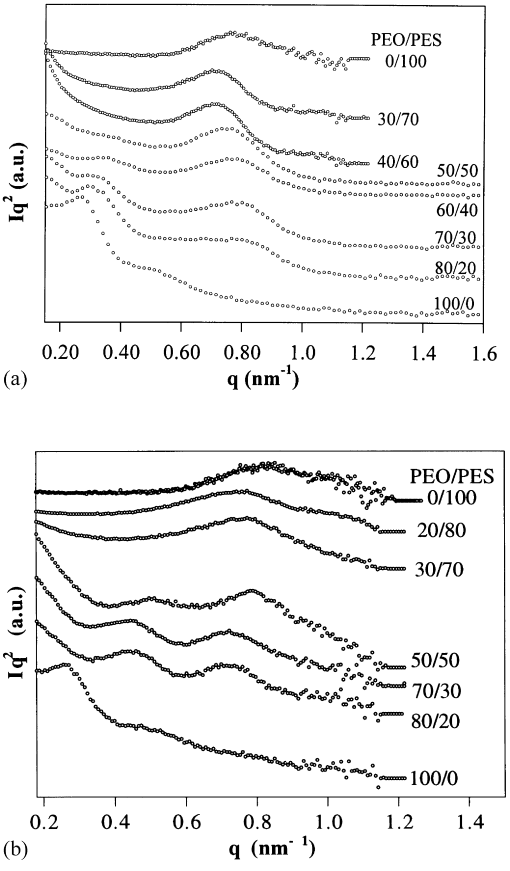

Fig. 9. Room-temperature Lorentz-corrected SAXS profiles of PEO/PES treated by: (a) two-step crystallization, direct cooling to 70°C followed by cooling to room temperature (ca. 27°C); and (b) one-step crystallization, direct cooling to 40°C.

cooled directly to 40°C to allow simultaneous crystallization of PEO and PES. A scattering peak at ca. 0.78 nm^{-1} is identified for all compositions. This peak position almost coincides with that of neat PES, indicating the existence of LS domains consisting of almost pure PES lamellae. Two scattering peaks are identified for PEO-rich blends, which verifies the presence of two separate LS domains. The zero-angle scatterings are again observed in all profiles for the blends. The zero-angle scattering is now associated with the electron density contrast between the two types of LS domains. The lower-q peak was not resolved for PES-rich blends owing to its small size and overlap with the zero-angle scattering.

In the case of PEO-rich blends, the lower-q peaks are located at ca. 0.44–0.5 nm^{-1} for one-step crystallization and at ca. 0.3–0.35 nm^{-1} for two-step crystallization. These peaks are located in between the peak position of neat PES and that of neat PEO (0.25 nm^{-1}), so they correspond to the LS domain consisting of mixed PEO and PES lamellae. The crystalline/crystalline morphology induced by both crystallization histories was thus represented by two separate LS domains, one contained almost pure PES lamellae and the other consisted of mixed PEO and PES lamellae.

It was suggested for one-step crystallization that PEO acted as a "temporary amorphous diluent" with respect to PES and was expelled interfibrillarly. As PEO was expelled into the interfibrillar zones containing the miscible mixture of PEO and PES, it enriched the PEO content within these regions and subsequent crystallization of PEO and PES within the more space-constrained interfibrillar regions may create the LS domains containing mixed PEO and PES lamellae. It should be noted that when the crystalline /crystalline state with dual LS domains was heated to 68°C, the PEO crystals in the mixed-lamellae domains were melted, leaving the PES lamellae within the prior mixed-lamellae domains. Therefore, the aforementioned "large individual amorphous domains" giving rise to the zero-angle scattering in Fig. 6 should be more accurately described as the domains consisting of amorphous PEO and PES lamellae. Upon melting the PEO crystals at 68°C, the long period associated with the prior mixed-lamellae domains should increase, so that the original lower-q peak should shift further to a lower angle. Such a low-q peak was however not resolved in the high-temperature profiles in Fig. 6 as it was masked by the zero-angle scattering.

As to two-step crystallization, since PEO was also expelled into the interfibrillar regions at 70°C, subsequent crystallization of PEO at room temperature may also yield a mixed-lamellae domain. The lower-q peaks of the blends treated by two-step crystallization located closer to the peak position of neat PEO (the difference in q_{max} is 0.05–0.1 nm^{-1} comparing with 0.19–0.25 nm^{-1} for one-step crystallization). This implies the mixed-lamellae domains generated by the two-step crystallization was composed of less PES lamellae. In other words, two-step crystallization has induced more effective separation for PEO and PES. The morphological characterizations presented here indicate that PEO/PES in the crystalline/crystalline state exhibit block lamellar arrangement, with one LS domain containing almost pure PES lamellae and the other containing mixed PEO and PES lamellae. Such a morphological structure can be properly depicted by Fig. 1(d).

4. Conclusions

PEO/PES is a melt-miscible blend consisting of two crystalline constituents. Miscibility and the crystallizable nature of the two components offered effective routes to modify the crystallization kinetics as well as create rich morphological structure. The crystallization rate of PES was promoted by slight dilution with PEO ($w_{PEO} \leq 0.2$) due to enhanced segmental mobility upon blending. The depression in crystallization driving force became more dominant as the PEO content was further increased, which consequently led to reduction in PES crystallization rate. For the crystalline/amorphous state created by direct cooling to 70°C, and direct cooling to 40°C followed by heating to 68°C, SAXS studies revealed significant extent of interfibrillar segregation of amorphous PEO. In the crystalline/crystalline state generated by both one- and two-step crystallization, two separate lamellar stack domains were observed, where one contained almost pure PES lamellae and the other consisted of mixed PEO and PES lamellae. The lamellar arrangement in PEO/PES blends was thus characterized by the "block mode", in contrast with the insertion mode in PC/PCL blends.

Acknowledgements

This work is supported by the National Science Council, ROC, under grant NSC 88-2216-E-007-014.

References

[1] Stein RS, Khambatta FB, Warner FP, Russell T, Escala A, Balizer E. J Polym Sci, Polym Symp 1978;63:313.
[2] Cheung YW, Stein RS. Macromolecules 1994;27:2512.
[3] Cheung YW, Stein RS, Lin JS, Wignall GD. Macromolecules 1994;27:2520.
[4] Song HH, Stein RS, Wu D-Q, Ree M, Philips JC, Legrand A, Chu B. Macromolecules 1988;21:1180.
[5] Tashiro K, Stein RS, Hsu SL. Macromolecules 1992;25:1801.
[6] Tashiro K, Izuchi M, Kobayashi M, Stein RS. Macromolecules 1994;27:1221.
[7] Tashiro K, Izuchi M, Kobayashi M, Stein RS. Macromolecules 1994;27:1228.
[8] Tashiro K, Izuchi M, Kobayashi M, Stein RS. Macromolecules 1994;27:1234.
[9] Tashiro K, Izuchi M, Kaneuchi F, Jin C, Kobayashi M, Stein RS. Macromolecules 1994;27:1240.

[10] Wignall GD, Londono JD, Lin JS, Alamo RG, Galante MJ, Mandelkern L. Macromolecules 1995;28:3156.
[11] Tashiro K, Imanishi K, Izumi Y, Kobayashi M, Kobayashi K, Satoh M, Stein RS. Macromolecules 1995;28:8477.
[12] Cheung YW, Stein RS, Wignall GD, Yang HE. Macromolecules 1993;26:5365.
[13] Cheung YW, Stein RS, Chu B, Wu G. Macromolecules 1994;27:3589.
[14] Avramova N. Polymer 1995;36:801.
[15] Penning JP, Manley RStJ. Macromolecules 1996;29:77.
[16] Penning JP, Manley RStJ. Macromolecules 1996;29:84.
[17] Fujita K, Kyu T, Manley RStJ. Macromolecules 1996;29:91.
[18] Liu L-Z, Chu B, Penning JP, Manley RStJ. Macromolecules 1997;30:4398.
[19] Avella M, Martuscelli E. Polymer 1988;29:1731.
[20] Avella M, Martuscelli E, Greco P. Polymer 1991;32:1647.
[21] Avella M, Martuscelli E, Raimo M. Polymer 1993;34:3234.
[22] Liu AS, Liau WB, Chiu WY. Macromolecules 1998;31:6593.
[23] Huo PP, Cebe P, Capel M. Macromolecules 1993;26:4275.
[24] Abe H, Doi Y, Satkowski MM, Noda I. Macromolecules 1994;27:50.
[25] Nojima S, Terashima Y, Ashida T. Polymer 1986;27:1007.
[26] Nojima S, Satoh K, Ashida T. Macromolecules 1991;24:942.
[27] Chen H-L, Hsiao M-S. Macromolecules 1998;31:6579.
[28] Schultz JM. J Polym Sci, Polym Phys Ed 1976;14:2291.
[29] Debye P, Bueche AM. J Appl Phys 1949;20:518.